[illegible]

YI JIN, SHOUPING WANG, JASON NACHAMKIN, AND JAMES D. DOYLE

Naval Research Laboratory, Monterey, California

GREGORY THOMPSON

NCAR, Boulder, Colorado

LEWIS GRASSO

CIRA, Fort Collins, Colorado

TEDDY HOLT, JON MOSKAITIS, HAO JIN, RICHARD M. HODUR, QINGYUN ZHAO, AND MING LIU

Naval Research Laboratory, Monterey, California

MARK DEMARIA

NOAA/NESDIS, Fort Collins, Colorado

(Manuscript received 6 February 2013, in final form 10 July 2013)

ABSTRACT

The impact of ice phase cloud microphysical processes on prediction of tropical cyclone environment is examined for two microphysical parameterizations using the Coupled Ocean–Atmosphere Mesoscale Prediction System–Tropical Cyclone (COAMPS-TC) model. An older version of microphysical parameterization is a relatively typical single-moment scheme with five hydrometeor species: cloud water and ice, rain, snow, and graupel. An alternative newer method uses a hybrid approach of double moment in cloud ice and rain and single moment in the other three species. Basin-scale synoptic flow simulations point to important differences between these two schemes. The upper-level cloud ice concentrations produced by the older scheme are up to two orders of magnitude greater than the newer scheme, primarily due to differing assumptions concerning the ice nucleation parameterization. Significant (1°–2°C) warm biases near the 300-hPa level in the control experiments are not present using the newer scheme. The warm bias in the control simulations is associated with the longwave radiative heating near the base of the cloud ice layer. The two schemes produced different track and intensity forecasts for 15 Atlantic storms. Rightward cross-track bias and positive intensity bias in the control forecasts are significantly reduced using the newer scheme. Synthetic satellite imagery of Hurricane Igor (2010) shows more realistic brightness temperatures from the simulations using the newer scheme, in which the inner core structure is clearly discernible. Applying the synthetic satellite imagery in both quantitative and qualitative analyses helped to pinpoint the issue of excessive upper-level cloud ice in the older scheme.

1. [illegible]

Impacts of cloud and precipitation processes on tropical cyclone (TC) development have been studied extensively using both observations and numerical models. Observations from field experiments and routine reconnaissance flights have led to detailed descriptions of the TC inner core structure and environment for mature TCs (Riehl and Malkus 1961; Gray and Shea 1973; Jorgensen 1984). The observed TC structure includes an outward-tilted eyewall laden with strong convection and updraft, radial inflow confined below 1.5–2 km, and outward-spiraling rainbands embedded within the stratiform rainfall region surrounding the eye. Latent heating in the

Corresponding author address: Yi Jin, Naval Research Laboratory, 7 Grace Hopper Avenue, Monterey, CA 93943-5502.
E-mail: yi.jin@nrlmry.navy.mil

DOI: 10.1175/MWR-D-13-00058.1

eyewall convection fueled by the enthalpy flux from the ocean is considered to play a major role in TC intensification (Malkus 1958; Malkus and Riehl 1960; Simpson et al. 1998; Willoughby 1998; Heymsfield et al. 2001; Zipser 2003). However, there have been limited direct observations of microphysical properties in TCs. Houze et al. (1992) documented ice and graupel mass and number concentration distributions at flight level (6 km above the surface) for Hurricane Norbert (1984). Their observations showed that small ice particles exist between the eyewall and outer rainbands, and graupel particles are collocated with the radius of maximum tangential wind. Observations of three Atlantic hurricanes investigated by Black and Hallett (1986) indicated that hurricanes are usually glaciated everywhere above the −5°C level and the stratiform areas are dominated by snowflakes (aggregates) at flight level. While no direct measurements were performed for the upper-level (about 300–200 hPa) cloud ice, the authors were able to deduce that most ice originates from ice multiplication processes (secondary ice production) in the eyewall updraft and is redistributed through the upper and midlevel outflows (~500 hPa). Recognizing the gap in hurricane cloud ice observations at upper levels, Heymsfield et al. (2006) conducted in situ and radar measurements for Hurricane Humberto (2001) to characterize ice microphysical properties at altitudes from 8.5 to 11.9 km (temperatures from −22° to −57°C). High concentrations of small ice particles were observed around and in the updraft, indicating homogeneous ice nucleation in the vicinity of the updraft. Two modes of ice size distribution were discovered, one for the ice particles in the eyewall updrafts and another in the stratiform areas.

Since the early 1960s the role of clouds and precipitation in TC intensity and inner-core structure changes have been investigated using numerical models with varying levels of complexity, ranging from idealized and/or axisymmetric simulations (Willoughby et al. 1984; Lord et al. 1984; Emanuel 1986, 1999; Hendricks et al. 2004; Willoughby 2009; Fierro et al. 2009) to three-dimensional models with full physical parameterizations (Kasahara 1961; Rosenthal 1978; Braun 2002; Wang 2002; Fovell et al. 2009; Liu et al. 1997; Zhu and Zhang 2006; Fierro et al. 2009; Shen et al. 2010). For example, numerical simulations using an axisymmetric nonhydrostatic TC model (e.g., Willoughby et al. 1984; Lord et al. 1984) suggest that inclusion of the ice phase in the microphysics parameterization results in a TC with very different structure. Because of the cooling effect of melting ice and graupel, the downdrafts are enhanced and the vortex growth rate is slower compared to those produced using liquid-water-only microphysics. The authors also recognized the uncertainty in parameterization of ice formation and its implication for snow growth from vapor deposition. Another idealized TC study by Fovell et al. (2009) suggested that average fall speed of hydrometeors could impact TC track forecasts through redistribution of the hydrometeors outward from the eyewall to anvil and modification of the environment via cloud–radiation interaction.

As more computing resources became available, numerical simulations at high resolution (1–3 km) using bulk microphysical schemes have proven useful (e.g., Rogers et al. 2007; Li and Pu 2008). The fine resolution has allowed analysis of detailed TC dynamics, such as the important contribution of hot towers (Hendricks et al. 2004) and the eyewall replacement cycle (Chen et al. 2011) to TC intensification/weakening. The success in TC numerical simulations, however, has been limited to individual cases. It remains a challenge for numerical weather prediction (NWP) models to produce reliable forecasts of TC intensity, in part because of the uncertainty in the representation of microphysical processes in the inner core and the storm environment (Rogers 2010). For example, the numerical models tend to overestimate graupel and the strength of updraft in the eyewall, as indicated in the study of Hurricane Erin (2001) by McFarquhar et al. (2006).

The majority of the high-resolution TC simulations make use of single-moment bulk microphysics schemes that predict only the mixing ratios (or mass content) of hydrometeors (cloud water, rain, ice, snow, graupel, etc.; Lin et al. 1983; Rutledge and Hobbs 1983; Schultz 1995; Reisner et al. 1998; Thompson et al. 2004; McFarquhar and Black 2004; McFarquhar et al. 2006). More recently, two-moment schemes have become available in numerical models (Ferrier 1994; Morrison and Pinto 2005; Milbrandt and Yau 2005). The additional computational cost for the second moment (e.g., number concentrations), however, hinders its applicability for operational NWP. The parameterization developed by Thompson et al. (2008, hereafter T2008) takes a different approach by predicting the number concentrations of cloud ice and rain, in addition to their mixing ratios, but continues to predict only mixing ratios of cloud water, snow, and graupel. This scheme deviates from many of the assumptions found in various schemes based on Lin et al. (1983). It incorporates findings from numerous field campaigns in an effort to reduce what has been noted by previous studies as a high-bias precipitation efficiency (Colle et al. 1999).

While the Thompson scheme has been examined extensively for winter storms (Liu et al. 2011; Molthan and Colle 2012) and other continental convective cases (Clark et al. 2012), this is its first application to TC cases as well as the basin-scale flow environment evaluation.

The Thompson scheme has been implemented recently in the Navy's Coupled Ocean–Atmosphere Mesoscale Prediction System for Tropical Cyclones (COAMPS-TC[1]), as part of the continuous effort by the Navy to improve TC prediction, in collaboration with the National Oceanic and Atmospheric Administration (NOAA) Hurricane Forecast Improvement Program (HFIP; http://www.hfip.org). In this paper the impact of the ice parameterization within the microphysical schemes on TC prediction is discussed through systematic forecast evaluation for both synoptic environment and TC cases. The remainder of the paper is organized into 4 sections. Section 2 provides an overview of the model and experimental setup. The impact of the two different microphysical parameterizations on the synoptic scale is discussed in section 3. The evaluation of TC track and intensity forecasts, including the application of synthetic satellite imagery, is presented in section 4. A summary and discussion of the implication of the results are given in section 5.

2.

COAMPS-TC is a new version of the Navy's operational regional model specifically designed to provide skillful predictions of TC track, intensity, and structure (Doyle et al. 2012). Data assimilation is accomplished through three-dimensional variational analysis, using the Navy Variational Data Assimilation System (NAVDAS; Daley and Barker 2001). NAVDAS performs quality control and assimilates all available observations (e.g., satellite data, soundings, aircraft measurements, buoy data, etc.). Additionally, TC synthetic observations are constructed from TC warning messages issued by the National Hurricane Center or Joint Typhoon Warning Center and assimilated by NAVDAS to enhance the TC inner core structure at the initialization time. A relocation method is applied during initialization to ensure that the preexisting TC circulation in the first-guess field is collocated with the observed TC center (Liou and Sashegyi 2012).

The forecast model uses terrain-following sigma-height coordinates and nonhydrostatic, fully compressible equations of motion following Klemp and Wilhelmson (1978). The Fu–Liou radiative transfer parameterization (Liu et al. 2009) is used for both shortwave and longwave radiation with a two-stream longwave configuration for computational efficiency. Cloud mass contents and effective radius are the two input variables required by the Fu–Liou scheme to compute cloud optics (e.g., optical depth, single scattering albedo, and asymmetry factor). Specific parameterizations are used to calculate cloud effective radius as functions of cloud mass. The choice of these parameterizations is based on extensive modeling studies of cloud–radiation interactions validated against observations from the Southern Great Plains Atmospheric Radiation Measurement Program. The surface layer parameterization follows Wang et al. (2002), which is a modified version of Louis (1979) and Fairall et al. (1996). The surface roughness has been modified to maintain a constant drag coefficient for winds stronger than $35\,m\,s^{-1}$ to reflect the recent findings from laboratory tank experiments (Donelan et al. 2004) and direct turbulence measurements at near-hurricane-force winds during the Coupled Boundary Layers Air–Sea Transfer (CBLAST) hurricane field experiment (Black et al. 2007). The boundary layer parameterization is a 1.5-order turbulence closure method (Mellor and Yamada 1982) where turbulent kinetic energy (TKE) is predicted explicitly. A physically consistent method is developed to include dissipative heating based on TKE dissipation to ensure energy conservation (Jin et al. 2007). The dissipative heating rate is applied at all levels, including the surface layer, in contrast to other studies in which dissipative heating is considered only at the surface due to the lack of TKE representation in layers above the surface.

To represent subgrid-scale convective processes, the Kain–Fritsch cumulus scheme (Kain and Fritsch 1990) is activated in domains with grid spacing greater than 10 km, while the microphysics parameterization is applied in all domains. The microphysics scheme used for the control simulations is a single-moment bulk scheme that predicts the mixing ratio of five microphysical species: cloud water, rain, cloud ice, snow, and graupel. This scheme is derived from Rutledge and Hobbs (1983) (called modified R-H hereafter), which in turn is similar to the Lin et al. (1983) treatment. Another recently implemented option in COAMPS-TC, the T2008 microphysical scheme, as described in the introduction, is used for the Thompson simulations. The comparison of the domain-averaged hydrometeors between the control and Thompson simulations (see section 3a for details) clearly indicated that the most significant difference between the two is in the ice amount at upper levels. Therefore, the focus of this study is on the ice-phase cloud microphysical processes.

COAMPS-TC simulations have been performed for 15 Atlantic basin TCs from 2010 and 2011with intensities varying from tropical storm (TS) to category 4 (cat-4) on the Saffir–Simpson hurricane scale (Table 1). Each forecast covers 120 h or the storm's life span, whichever is shorter. The model domain consists of three nests with 45-, 15-, and 5-km grid spacing for the

[1] COAMPS-TC is a registered trademark of the Naval Research Laboratory.

TABLE 1. List of TCs: storm names (numbers assigned by NHC), simulation periods (yyyymmddhh) followed by the best track storm lifetime maximum intensity category in parentheses, and the number of cases for each storm simulated. [Saffir–Simpson scale: cat-1: 74–95; cat-2: 96–110; cat-3: 111–130; cat-4: 131–155; and cat-5: >155 mi h^{-1} (1 mi h^{-1} = 0.4470 m s^{-1}); TS: 39–73 mi h^{-1}.]

Storm name (number)	Period	Number of cases
Bonnie (03L)	2010072212–2010072400 (TS)	4
Danielle (06L)	2010082118–2010083000 (Cat-4)	17
Earl (07L)	2010082512–2010090200 (Cat-4)	16
Igor (11L)	2010090812–2010091612 (Cat-4)	17
Julia (12L)	2010091212–2010092012 (Cat-4)	17
Lisa (14L)	2010092100–2010092612 (Cat-1)	12
Paula (18L)	2010101118–2010101500 (Cat-2)	7
Richard (19L)	2010102100–2010102612 (Cat-2)	12
Bret (02L)	2011071800–2011072012 (TS)	6
Irene (09L)	2011082212–2011082700 (Cat-3)	10
Katia (12L)	2011082912–2011090600 (Cat-4)	16
Maria (14L)	2011090700–2011091412 (Cat-1)	16
Ophelia (16L)	2011092106–2011100212 (Cat-4)	23
Philippe (17L)	2011092406–2011100600 (Cat-1)	24
Rina (18L)	2011102400–2011102712 (Cat-1)	8
Total: 15 storms	July–October of 2010 and 2011	Total: 205 cases

outer, intermediate, and inner domains, respectively (Fig. 1). The two inner nests move with the TC center. Two-way interaction is specified between the nested domains. Forty vertical levels are employed with the lowest model level at 20 m and the model top at 32 km.

3.

Basin-scale synoptic flow simulations were performed for the 6 August–30 September 2010 time period using the outer 45-km domain only. Each forecast was run to 120 h. The first forecast was initialized at 0000 UTC 6 August 2010 using the Navy Operational Global Atmospheric Prediction System (NOGAPS) forecasts as the first-guess fields (cold-start forecasts). Subsequent forecasts (cycled every 12 h) used the COAMPS-TC 12-h forecasts from the previous forecast, including clouds and precipitation, as the first guess (warm start). As such, any difference between the simulations using the modified R-H and Thompson microphysical schemes become increasingly evident for those forecasts initialized later during the 2-month period. Each forecast is 120 h long. The NOGAPS[2] forecasts were also used as boundary conditions. Focusing on the coarse grid—a different approach compared to many previous TC environmental studies that focused on individual cases—allows for a more systematic assessment of the impact of the two microphysical parameterizations on the synoptic-scale environment. The examined fields are averaged over the 2-month period as a function of forecast lead times. Additionally, averaged differences between forecasts and initial fields (e.g., averaged 300-hPa temperature changes at 120 h from 0 h) were derived to remove the base-state variations in the forecasts. In this section we first analyze cloud ice and upper-level temperature from simulations using the two parameterizations. The interaction between radiation and cloud ice is then illustrated. Several major differences between the two schemes related to the ice phase cloud treatment are also discussed.

a. Cloud ice and upper-level temperature

The most notable difference between the forecasts using the modified R-H and the Thompson microphysics lies in the amount of upper-level cloud ice. Figures 2a and 2b display the 250-hPa level cloud ice for the 120-h forecast averaged over all simulations during the nearly 2-month period. Cloud ice increases steadily with forecast lead time in the control and by the end of the 120-h forecast most of the domain is covered by cloud ice with a domain mean of 0.03 g kg^{-1} and a maximum value of 0.5 g kg^{-1} (Fig. 2a). In contrast the Thompson simulations produced much less cloud ice (Fig. 2b). The domain mean cloud ice of 0.003 g kg^{-1} and maximum of 0.01 g kg^{-1} are an order of magnitude smaller than those from the control. The cloud ice is seen mainly in the layer between 350 and 150 hPa (not shown) with the maximum near 250–200 hPa.

Associated with the widespread cloud ice distribution at upper levels, cooling of up to 1°C occurs at 100 hPa near the top of the cloud ice layer and significant warming near the base of the cloud ice layer. The 300-hPa level temperature change between the 120-h forecast and the initial time averaged over the nearly 2-month period shows positive values over the most of the domain for the control (Fig. 3a) and exceeds 2°C over areas where cloud ice mixing ratios are above 0.06 g kg^{-1}. The warming is confined to a much smaller area in the Thompson simulations (Fig. 3b).

The difference between the two microphysical schemes is also evident in the change of 500-hPa geopotential heights, which directly impacts the TC steering flow (Chan and Gray 1982). The Thompson simulations have an ~(10–20)-m increase in heights over the subtropical regions (20°–35°N, 110°–50°W) during this period (Fig. 4b), whereas the control simulations display

[2] GFS forecasts were not stored for the entire synoptic simulation period. Comparisons between the simulations using NOGAPS and GFS when the GFS data were available suggest that our conclusions based on the synoptic simulations forced by NOGAPS are consistent with those forced by GFS.

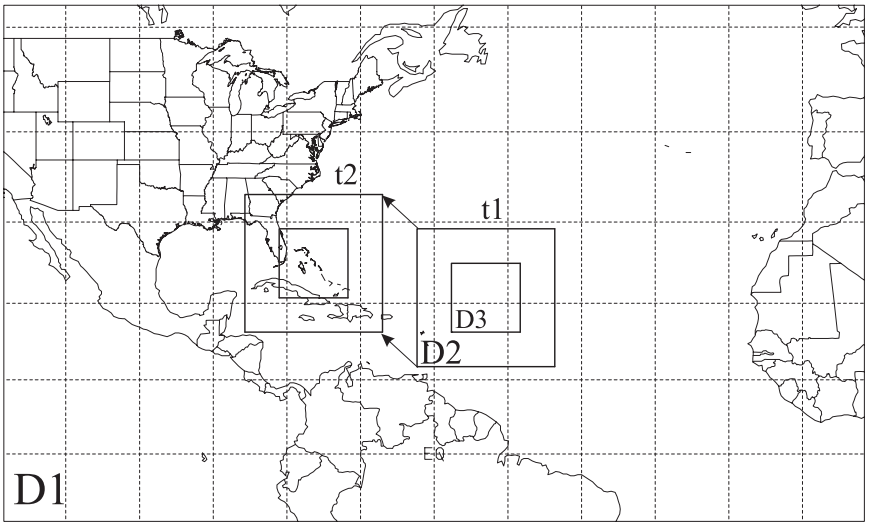

FIG. 1. Domains used for the numerical experiments. The inner two nests follow the storm and can be centered at different locations at different times (t1 vs t2 in the figure); the arrows indicate the moving direction of the inner nests. The synoptic simulations were performed for the outer domain (D1) only.

up to a 20-m reduction in the heights over the same area (Fig. 4a). Consequently the southern edge of the subtropical high in the control simulations retreats northward so that the 5890-m contour shifts from south of Cuba and Hispaniola at the initial time to north of these islands after 120 h (Fig. 4a). This northward retreat of the subtropical high is associated with the large rightward cross-track bias in TC track forecasts in the control simulations (see section 5). The average 5890-m contour in the Thompson simulations remains nearly stationary through 120 h (Fig. 4b) and the forecast tracks experience less rightward cross-track error. The results are consistent with the relationship between the subtropical high and TC tracks that has long been recognized over the western North Pacific (Chan et al. 2001; Wu et al. 2007; Chen et al. 2009), in that TC tracks are influenced by the southward expansion of the subtropical high via large-scale steering flow.

Upper-level cloud ice forms mainly through ice nucleation, which depends on the presence of ice nuclei (IN). Aerosol particles (AP) act as IN under most atmospheric conditions in four major modes: deposition, condensation freezing, immersion, and contact freezing. Any given AP of a certain size and chemical composition can be IN for any one or all four modes of nucleation (Pruppacher and Klett 1978). The complexity of the ice nucleation processes and massive spread in observed ice number concentrations (DeMott et al. 2011) lead to large uncertainties in representing IN and their complex interactions with the atmospheric environment in NWP models, as evidenced by nearly a dozen different formulations for numbers of ice crystals (NI) employed in the microphysical schemes (Meyers et al. 1992; Hong et al. 2004; Thompson et al. 2004; T2008). Two of the most frequently used formulations are based on the research of Fletcher (1962) and Meyers et al. (1992), which are expressed as functions of temperature and/or ice supersaturation:

Fletcher:

$$N_{i,\text{Fletcher}} = 10^{-2} \exp[0.6(T_0 - T)], \tag{1}$$

Meyers:

$$N_{i,\text{Meyers}} = \exp(-0.639 + 0.1296 S_i), \tag{2}$$

where $T_0 = 273.15$ K, T is the ambient air temperature (K), S_i is the supersaturation (%) with respect to ice, and N_i is the number of ice crystals initiated (m^{-3}). The observed NI counts at a dozen locations worldwide, from which the Fletcher formulation was derived, vary by more than an order of magnitude between locations, underscoring the variability of NI characteristics. The Cooper (1986) formulation was based on in situ measurements of ice crystals in continental clouds and was adopted for use in the T2008 scheme primarily because of the reduced number of ice crystals at temperatures at which supercooled water frequently exists (0° to −15°C):

Cooper:

$$N_{i,\text{Cooper}} = 5.0 \exp[0.304(T_0 - T)]. \tag{3}$$

The Cooper formulation produces as much as two orders of magnitude more NI at warmer temperatures

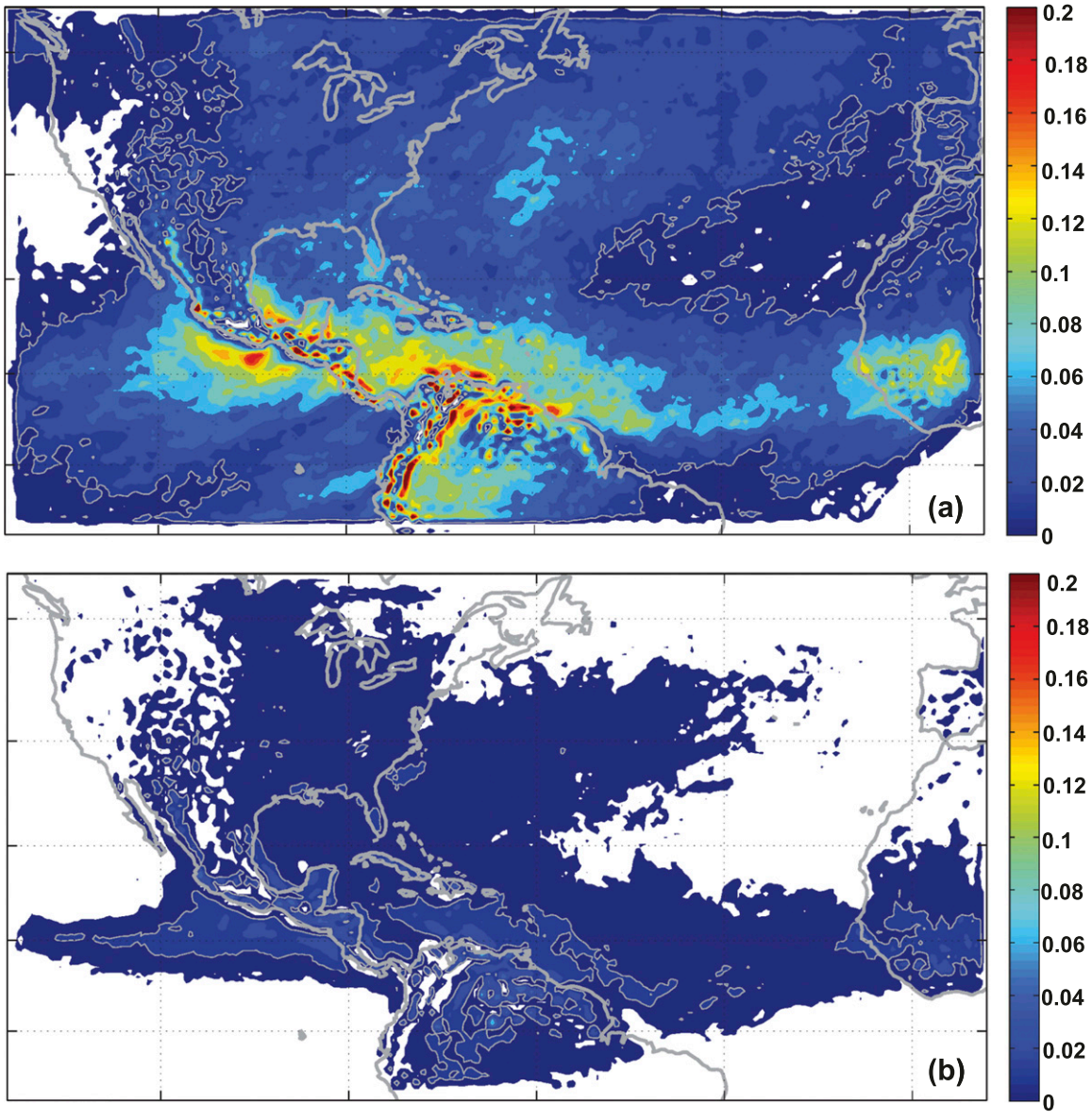

FIG. 2. COAMPS-TC forecast 250-hPa level cloud ice (g kg^{-1}) at forecast hour 120 averaged over all simulations every 12 h from 6 Aug to 30 Sep 2010 in domain D1 from (a) the control simulations and (b) the Thompson simulations.

(>−20°C) than Fletcher's, whereas Fletcher's has more than an order of magnitude more NI at colder temperatures (Fig. 5a). The NI formulation used by the modified R-H scheme follows Fletcher's curve at colder temperatures. A sensitivity test (see Cooper in Table 2) was designed to replace the NI formulation in the modified R-H microphysical scheme with the Cooper formulation. The experiment was exactly the same as the control except it was cycled for a 2-day period from 0000 UTC 6 August to 0000 UTC 7 August 2010 since the impact of the changes on the cloud and temperature distributions became consistently evident by this time. Additionally, the simulations with no cloud–radiation interaction (i.e., the no-ice-rad test) would deviate from reality significantly if cycled for more than a few days.

Using the Cooper formulation effectively reduces the upper-level cloud ice (the magenta line in Fig. 5b), so that the domain-averaged 300-hPa temperature increase with time is less than 0.5°C (the magenta line in Fig. 5c), compared to the >1°C increase seen in the control (the blue line in Fig. 5c). The horizontal distribution of cloud ice from the Cooper experiment at 120 h (Fig. 6c) is generally one order of magnitude less than that in the

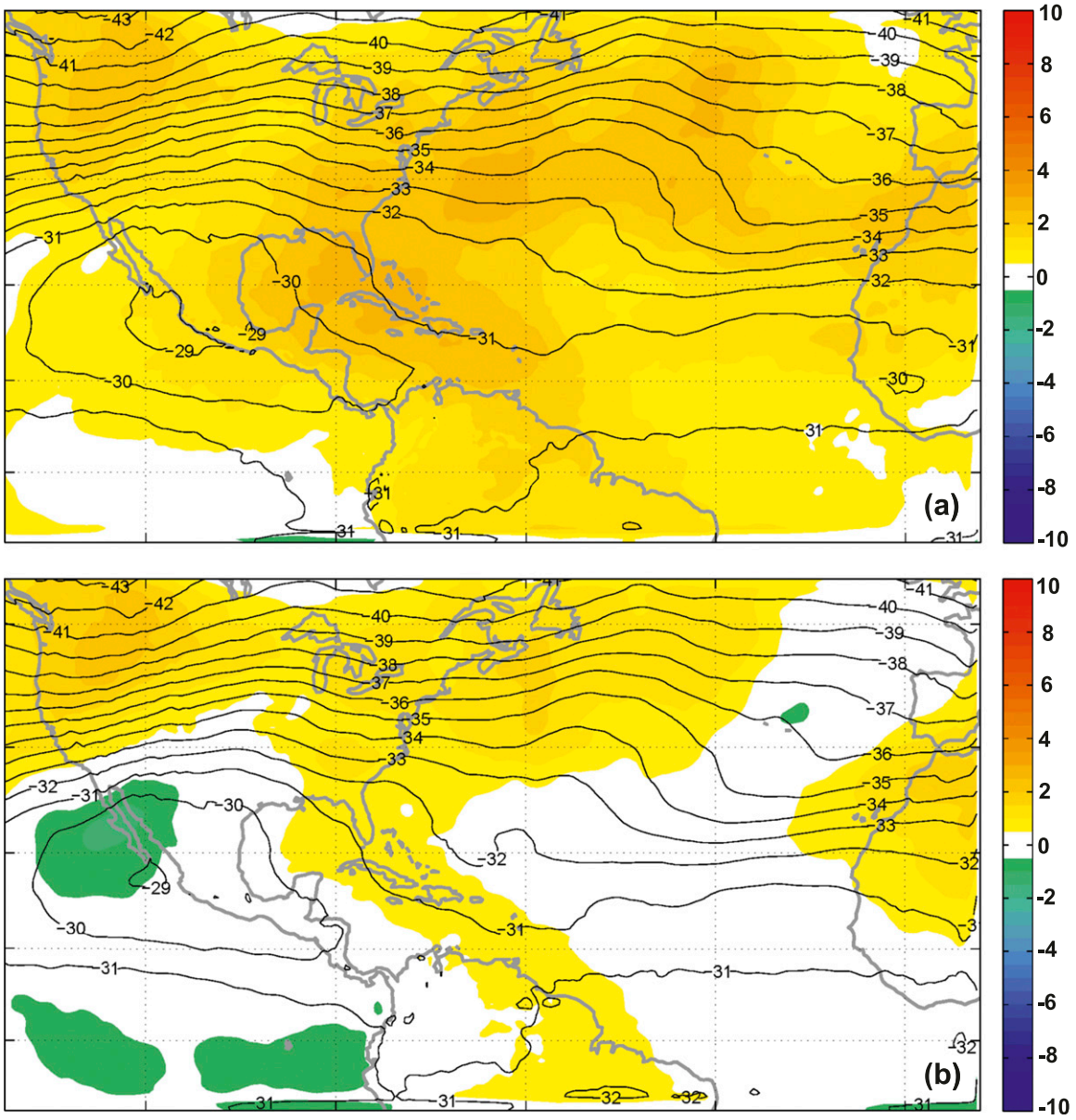

FIG. 3. As in Fig. 2, but for 300-hPa level temperature change (°C, shading) between the 120-h forecast and the initial time. The contours are averaged temperature (contoured at 1°C) at 0 h.

control experiment (Fig. 6a) but similar to the amount simulated using the Thompson scheme (Fig. 6b), which is not surprising given that the Cooper formulation is also used in Thompson. The upper-level warming tendency during the forecast is reduced substantially so that the temperature difference at 120 h between the Cooper test and the control simulation (Fig. 7b) is very close to the difference between the Thompson simulation and control simulation (Fig. 7a). The 120-h forecast temperature is reduced by >1°C over the subtropical Atlantic area in both the Thompson and Cooper simulations compared to the control simulations. The Thompson scheme adopted the Cooper formulation because the Fletcher formulation produced erroneously large amount of cloud ice at the upper levels for their winter precipitation cases (T2008).

It should be pointed out that the characterization of ice and snow is a modeling artifact, which is dealt with differently between the two schemes. The Thompson scheme converts ice crystals of diameters >200 μm into snow. By contrast, the autoconversion from ice to snow in the modified R-H scheme does not happen

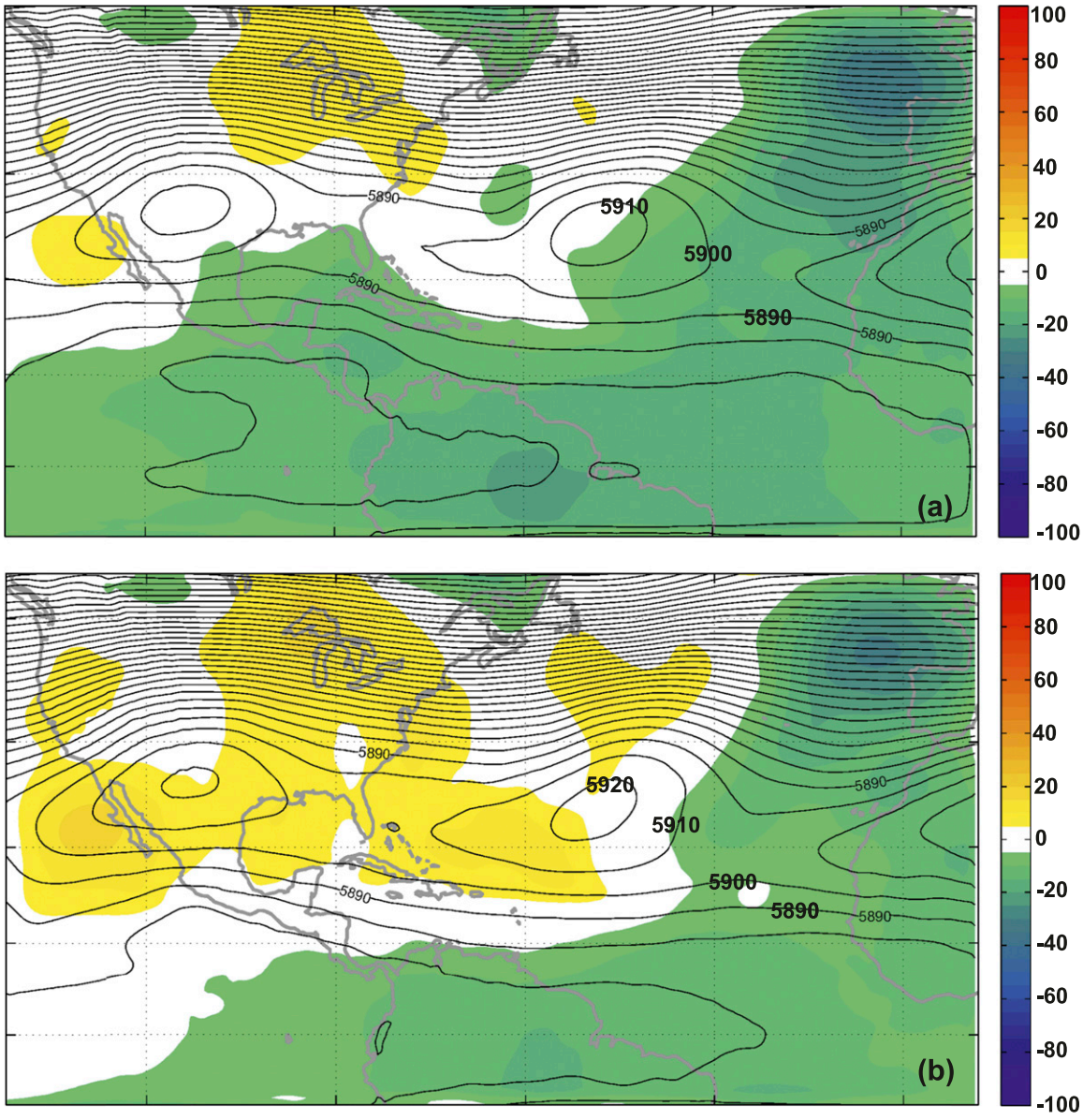

FIG. 4. As in Fig. 3, but for 500-hPa level geopotential heights (contoured at 10-m intervals) and 500-hPa level geopotential height change (shading).

until the mass of the ice crystal exceeds the threshold corresponding to crystal with diameters greater than 500 μm. (Table 3). A more complete picture describing domain-averaged hydrometeors generated by the two schemes is shown in Fig. 8. The domain-averaged cloud ice from the control simulation reaches 0.03 g kg^{-1} at ~250 hPa, whereas the Thompson simulation has a maximum value of ~0.0025 g kg^{-1}, one order of magnitude less. On the other hand, the control simulation produced snow in a layer between 650 and 250 hPa with a maximum of ~0.007 g kg^{-1} at 400 hPa. The Thompson scheme is efficient in converting ice particles to snow and produced snow at levels as high as 100 hPa, with a maximum of nearly 0.01 g kg^{-1} at ~350 hPa. The sum of the snow and ice at upper levels from the Thompson simulation, however, remains about only one-third of that from the control simulation. Moreover, the horizontal distribution of the sum of snow and ice (not shown) displays similar comparison to that for ice alone (Fig. 6). Therefore, the results presented for cloud ice remain valid even given the varying methods distinguishing ice and snow between the two schemes.

The distribution of the liquid cloud is similar between the two schemes in general although a small amount of

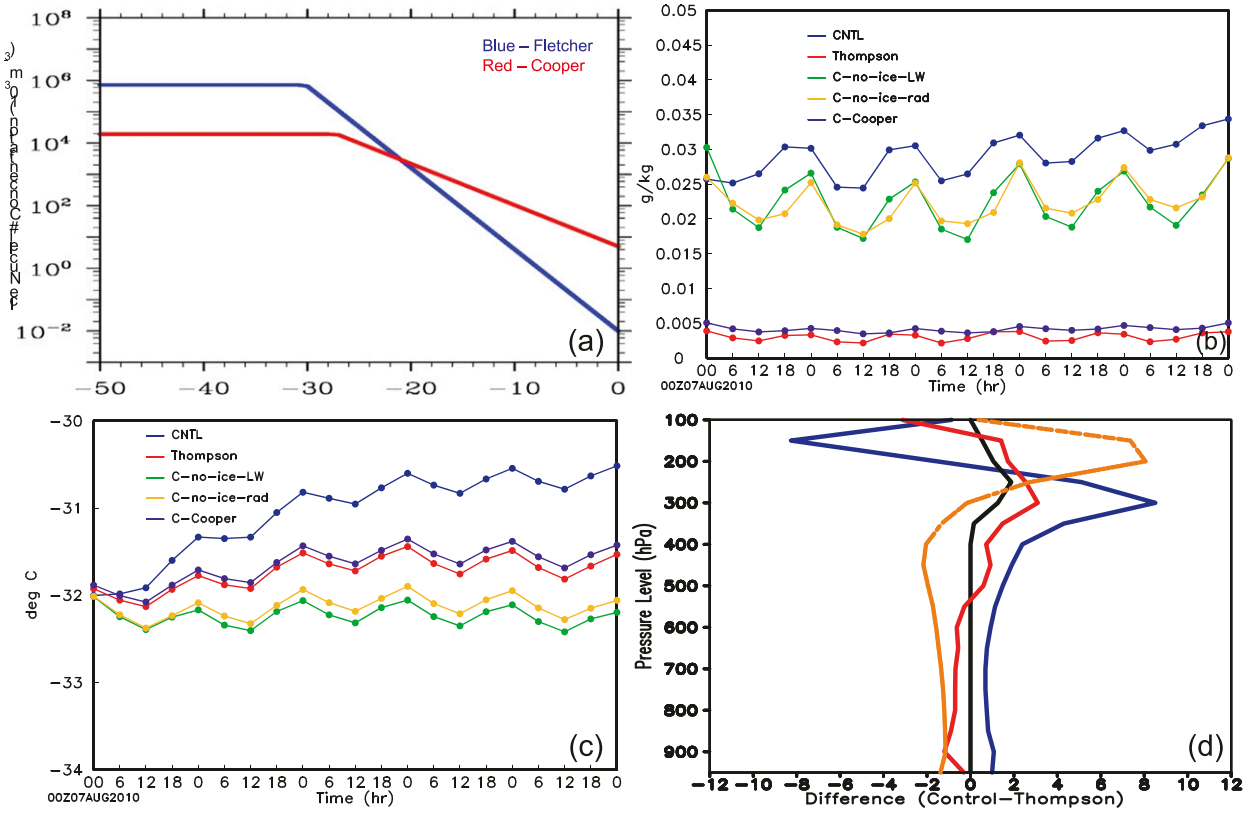

FIG. 5. (a) Number concentration of (pristine) ice crystals (10^3 m^{-3}) as a function of temperature from the Fletcher (blue) and Cooper (red) formulations. (b) COAMPS-TC forecast domain-average 250-hPa cloud ice mixing ratio (g kg^{-1}) evolution during the 120 h of the synoptic simulation initialized at 0000 UTC 7 Aug 2010: the control (blue), Thompson (red), Cooper (magenta), no-ice-lw (green), and the no-ice-rad (yellow) experiments (see Table 2 for descriptions of the sensitivity experiments). (c) As in (b), except for the 300-hPa temperature (°C). (d) Vertical profiles of differences between the control and Thompson experiments (control − Thompson) at 20°N, 60°W for longwave radiative heating rates (K day^{-1}) (blue), shortwave radiative heating rates (K day^{-1}) (orange dashed), cloud ice mixing ratio (0.1 g kg^{-1}) (black), and temperatures (°C) (red).

cloud water exists in a deeper layer (up to near 400 hPa) from the Thompson scheme than the modified R-H scheme. In the boundary layer (between 1000 and 900 hPa) the Thompson scheme has about 40% more cloud water than the modified R-H. Because of the coarse resolution in the 45-km domain, the convection remains weak for both simulations and hence the rain mixing ratio is quite small and amounts of graupel are negligible.

b. *Other differences related to ice phase cloud treatment*

In the Thompson scheme ice does not initiate until the water vapor mixing ratio reaches 25% supersaturation with respect to ice for temperature greater than −25°C. Our sensitivity tests with and without this constraint (the satv_ice test in Table 2) in the Thompson scheme does not show substantial differences in the upper-level cloud

TABLE 2. List of synoptic simulations performed with 12-h update cycles and the 120-h duration for each simulation.

Experiment name	Period (yyyymmddhh)	Main features
Control	2010080600–2010093012	Modified R-H microphysical scheme
Thompson	2010080600–2010093012	T2008 microphysical scheme
Cooper	2010080600–2010080700	Modified R-H with Cooper NI formulation
No-ice-lw	The same as Cooper	Modified R-H with ice and longwave radiation interaction disabled
No-ice-rad	The same as Cooper	Modified R-H without ice–radiation interaction
Satv_ice	The same as Cooper	Thompson with the ice saturation criteria change (see section 3b for details)

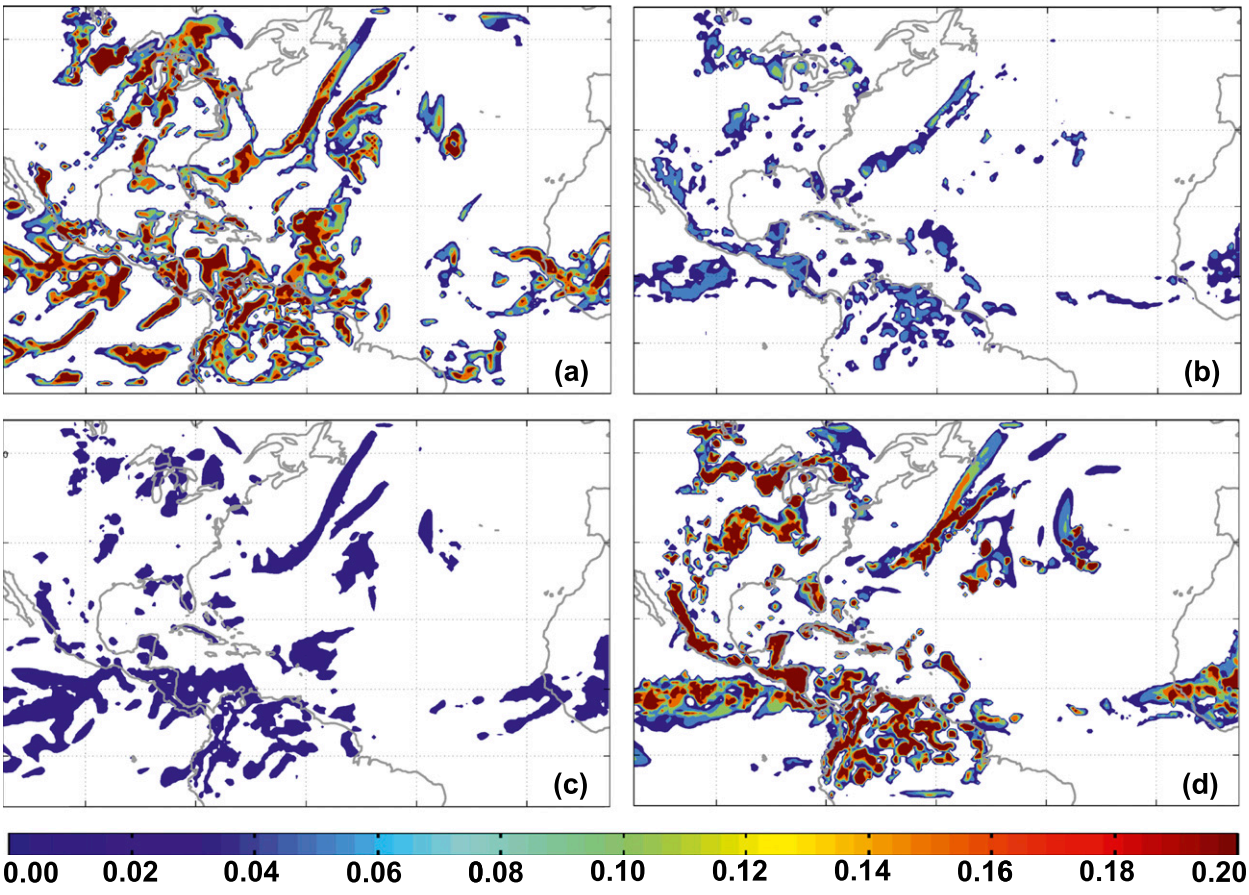

FIG. 6. (a) COAMPS-TC forecast 250-hPa cloud ice mixing ratio (g kg^{-1}) at 120 h for the synoptic simulations initialized at 0000 UTC 7 Aug 2010 from experiments (a) control, (b) Thompson, (c) Cooper, and (d) no-ice-rad.

ice. This result is expected since the ice supersaturation threshold change affects ice initiation at relatively low levels where the temperatures is much greater than is found in the upper troposphere.

Several other differences related to the cloud ice treatment are worth mentioning as well (Table 3). As a two-moment scheme, the Thompson scheme predicts both the mixing ratio and number concentration of ice crystals. Numerous sinks–sources are considered for ice crystals in the Thompson scheme, whereas the modified R-H scheme uses the NI formulation to diagnose the ice crystal number at each time step.

Another notable difference between the two schemes is the terminal velocity of the ice crystals (V_{ti}). The Thompson scheme follows the V_{ti} formulation of Ferrier (1994):

$$V_{\text{ti-T}}(D) = \left(\frac{p_o}{p}\right)^{1/2} \alpha D^{\beta} e^{-fD}, \tag{4}$$

where $p_o = 1013.25$ hPa, p is pressure, and D is the diameter of ice particles. Using the values listed in Table A1 of T2008, Eq. (4) is reduced to

$$V_{\text{ti-T}}(D) = 1847.5\left(\frac{p_o}{p}\right)^{1/2} D. \tag{5}$$

The modified R-H scheme uses a similar formulation with different coefficients (Cotton and Anthes 1989). For example, for ice particles with diameters $<212\ \mu$m,

$$V_{\text{ti-C}}(D) = 304.0\left(\frac{p_o}{p}\right)^{1/2} D. \tag{6}$$

Note that the 212-μm diameter limit here is close to the 200-μm threshold used by the Thompson scheme to convert ice to snow. For the frozen particles considered as ice by both schemes $V_{\text{ti-T}}$ is ~6 times larger than $V_{\text{ti-C}}$ for particles with the same diameter. A sensitivity test was performed by replacing $V_{\text{ti-C}}$ with $V_{\text{ti-T}}$ in the modified R-H scheme. The domain-averaged cloud ice amount from this test is only slightly (<5%) less than that from the control simulation. Further tests on varying the ice deposition rate and ice-to-snow autoconversion rate in the modified R-H scheme revealed minimal impact on

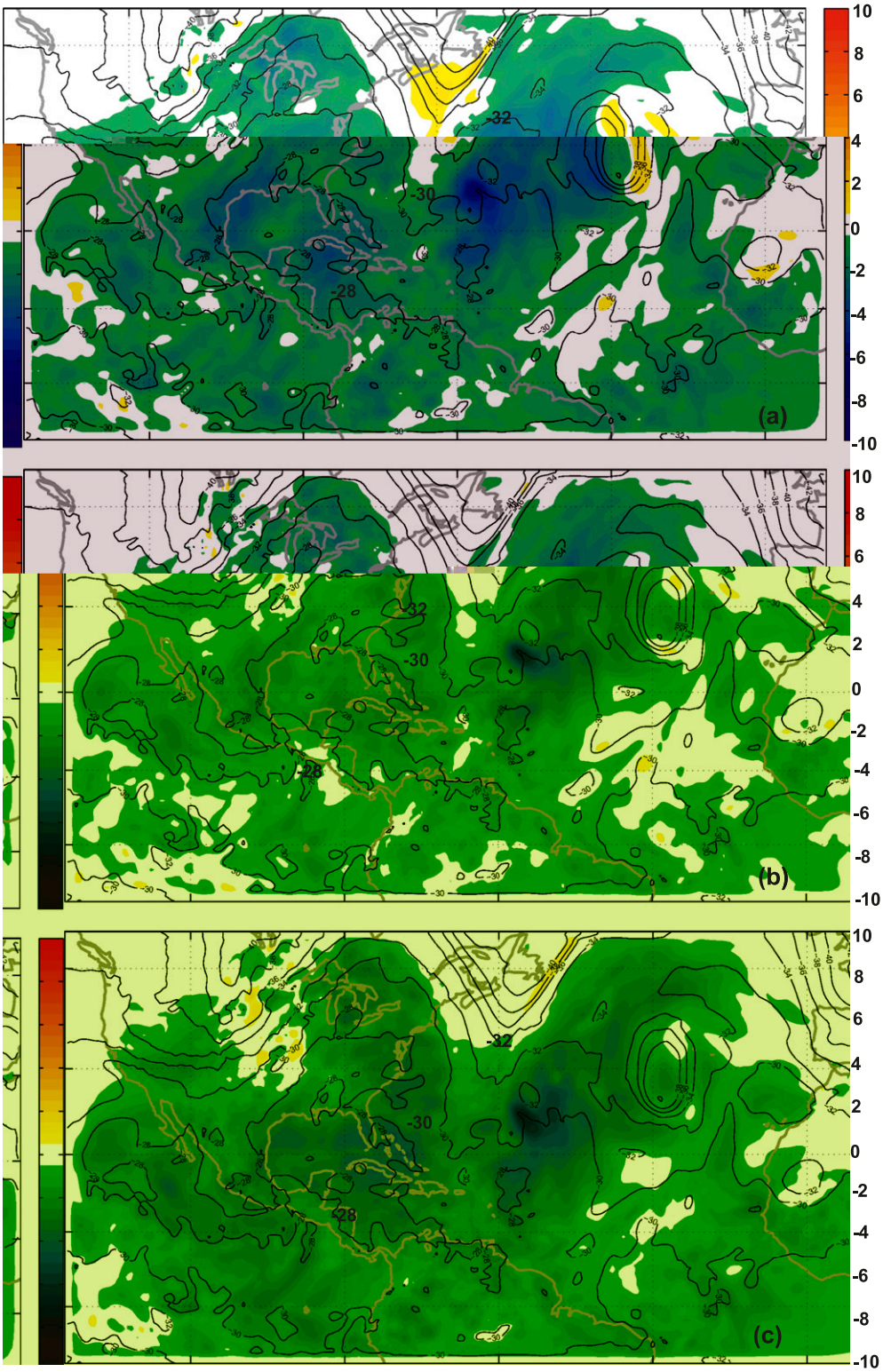

FIG. 7. (a) COAMPS-TC forecast 300-hPa temperature difference (°C, shading) between the Thompson experiment and the control experiment (Thompson − control) at 120 h for synoptic simulations initialized at 0000 UTC 7 Aug 2010. The contours (every 2°C) are for the 300-hPa temperature at the initialization time. (b),(c) As in (a), but for the Cooper and the no-ice-rad experiments, respectively .

TABLE 3. Some major differences in the treatment of ice phase clouds between the modified R-H and Thompson schemes.

Schemes	Ice nucleation	Ice crystal number concentration	Ice deposition growth	Threshold for autoconversion from ice to snow	Ice particle terminal velocity
Modified R-H	Fletcher (1962)	Diagnostic (see text)	Linear function of ice supersaturation [Eq. (A18) of RH83]	Ice particle mass (a value corresponding to a particle with 500-μm diameter)	Mass weighted following Cotton and Anthes (1989)
Thompson	Cooper (1986)	Prognostic (see text)	Cubic polynomial function of ice supersaturation [Eq. (C1) of T2008]	Ice particle diameter (200 μm; T2008)	Mass weighted (T2008) (see text)

the cloud ice amount. The difference in the ice nucleation remains the dominant cause for the difference seen in the upper-level cloud ice between the two schemes.

c. *Cloud ice–radiation interaction*

In an attempt to diagnose the physical processes responsible for the tropospheric warming in the control simulations, we performed two additional sensitivity tests. The no-ice-lw test (Table 2) is similar to the control simulations, except that the interaction between the cloud ice and longwave radiation is disabled, whereas the no-ice-rad test removes the interaction between cloud ice and both longwave and shortwave radiation. The domain-average cloud ice from those two sensitivity tests (the green and yellow lines in Fig. 5b) is close to the cloud ice amount from the control experiment and remains an order of magnitude higher than those in the Thompson and Cooper experiments. Despite the high values of cloud ice, the 300-hPa average temperatures show no warming trend with forecast lead time, hovering around −32.3°C, a value even lower than those from the Thompson and Cooper experiments (Fig. 5c). These two tests demonstrate the important contribution of cloud–radiation interaction to the upper-level warming. Furthermore, the temperature difference between the control simulation and the no-ice-lw, which reaches 1.5°C at 120 h, is much higher than the difference between the no-ice-lw and no-ice-rad (~0.1°C). This comparison indicates that the longwave radiation and cloud ice interaction plays a more dominant role than the shortwave and cloud ice interaction in the 300-hPa warming.

The cloud–radiation interaction can be further illustrated in vertical profiles of the difference fields between the control and Thompson simulations (Fig. 5d) for a selected point (20°N, 60°W) at 114 h corresponding to 1100 local time. The large difference in the cloud ice mixing ratio between the two experiments (control − Thompson), with a maximum of 0.2 g kg^{-1} at ~250 hPa (the black line in Fig. 5d), is due solely to the large amount of ice generated in the control experiment. An up to 7°C day^{-1} longwave radiative warming rate occurs in the control experiment near the base of the cloud ice

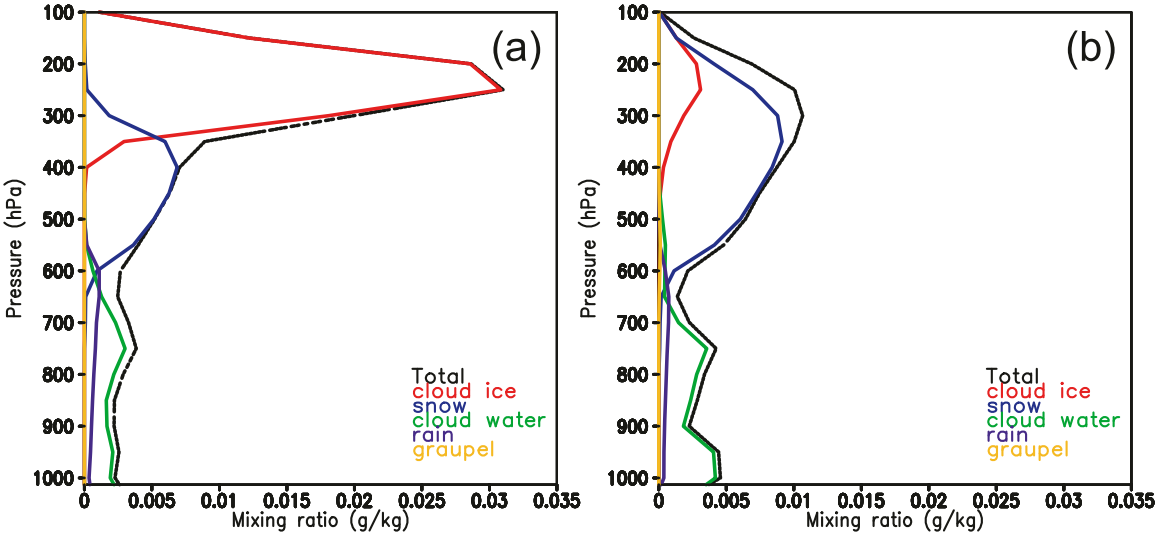

FIG. 8. Vertical profiles of domain-averaged hydrometeor mixing ratios: cloud water (green), rain (blue), ice (aqua), snow (blue), graupel (red), and the sum (black) for COAMPS-TC 120 h forecast in D1 valid at 0000 UTC 12 Aug 2010 from (a) the control and (b) the Thompson simulations.

layer at about 350–250 hPa with the maximum at 300 hPa. To the contrary, the Thompson experiment produced a longwave cooling of up to 1.5°C day^{-1} in the absence of cloud ice, resulting in an ~8.5°C day^{-1} difference between the two at 300 hPa (the blue line in Fig. 5d). The air temperature difference between the two experiments is ~3°C at 300 hPa. This warming near the base of cloud ice is caused by the localized large convergence of the upward longwave radiation flux due to a large difference between the temperature at the cloud base and at the surface (Nicholls 1984). Substantial differences are also seen in the longwave radiative cooling near the top of the cloud ice layer, which is mainly compensated for by the solar radiative warming (the dashed line in Fig. 5d).

4.

The impact of the microphysical scheme on TC prediction is evaluated in this section. The experimental design is similar to the real-time COAMPS-TC forecasts performed over the past three years (Doyle et al. 2012), with the three nests of 45-, 15-, and 5-km grid spacing for the outer, intermediate, and inner domains, respectively (Fig. 1). For each storm, the initial forecast is cold started using the National Centers for Environmental Prediction's (NCEP's) Global Forecast System (GFS) output as the first guess. Subsequent forecasts are warm started, using the COAMPS-TC 6-h forecasts from the previous forecast as the first guess. NAVDAS is used to assimilate observations every 6 h, and all forecasts use 6-hourly GFS forecasts for lateral boundary conditions.

a. Synthetic satellite imagery of Hurricane Igor

The evaluation of the model simulations thus far has been focused on the comparison of the various synoptic-scale simulations. In this section we use satellite observations and synthetic satellite imagery to evaluate the model simulations at both the synoptic and convection-resolving scale for Hurricane Igor (2010). The synthetic imagery, described in Grasso et al. (2008) and Bikos et al. (2012), provides a unique means of model evaluation, especially over open oceans where observations are scarce. The COAMPS-TC forecast hydrometeors (cloud droplets, rain, ice, snow, and graupel) and thermodynamic fields (e.g., pressure, temperature, and humidity) are used as inputs for a forward radiative transfer model to compute radiances for various spectral bands to derive brightness temperatures that the *Geostationary Operational Environmental Satellite (GOES)-13* would observe. Specifically, imagery from the 6.48-μm water vapor channel [channel 3 (CH3)] and the 10.7-μm infrared channel [channel 4 (CH4)] are analyzed. The *GOES-13* observations of roughly 4–8-km original resolution have been interpolated to the model grids using a nearest neighbor algorithm.

Igor was the strongest hurricane of the 2010 Atlantic season with maximum surface sustained winds reaching 130 kt (1 kt = 0.5144 m s^{-1}) on 13 September (see http://www.nhc.noaa.gov/pdf/TCR-AL112010_Igor.pdf). At 0000 UTC 14 September 2010 the brightness temperatures (Tb) from CH3 and CH4 clearly show low Tb from convection associated with Igor east of the Caribbean (Figs. 9a,b). Also depicted are two other major areas of convection: one associated with a persistent deep-layer trough off the northeastern U.S. coast and another over Cuba and the Caribbean Sea. The synthetic imagery from the 120-h forecast for the control simulation (Figs. 9c,d) in the outer domain, while capturing the convection over the three areas mentioned above, displays wide areas of much colder Tb than the observed, due to the widespread upper-level cloud ice coverage. The convective region associated with the hurricane becomes indistinguishable under the thick cloud ice for both channels. The Tb structure in the synthetic imagery from the 120-h forecast for the Thompson simulation, on the other hand, resembles the general distribution of convection over the northeastern United States and over Hurricane Igor (Figs. 9e,f). The convection over Cuba is not represented in the Thompson simulation, presumably due to the low resolution in this outer domain (D1).

In the innermost 5-km nest the strong convection in the eyewall region is well differentiated by the Thompson experiment, as indicated by the low Tb values of <213 K (Figs. 10e,f). Further comparison of the imagery shows a ~50% wider eye in Thompson than was observed (Figs. 10a,b). The Thompson experiment did not produce a symmetric, tight eyewall as observed, possibly because the simulated hurricane was less intense than observed, or perhaps due to the marginal resolution of the 5-km grid to reproduce these small-scale features. The forecast displays some indication of the convective band to the east and southeast of the storm center. The eyewall convection in the control simulation, however, is masked severely by the widespread cloud ice (Figs. 10c,d), which prevents further comparison with the observed inner core structure using this method.

Both the synoptic simulations and the qualitative Tb comparison for the Igor case have shown that the Thompson scheme reduces the upper-level cloud ice bias significantly. Furthermore, a quantitative evaluation of the synthetic CH4 Tb distribution was performed in D1. Depicted in Fig. 11a is the areal coverage of model forecast Tb at 120 h compared with the satellite

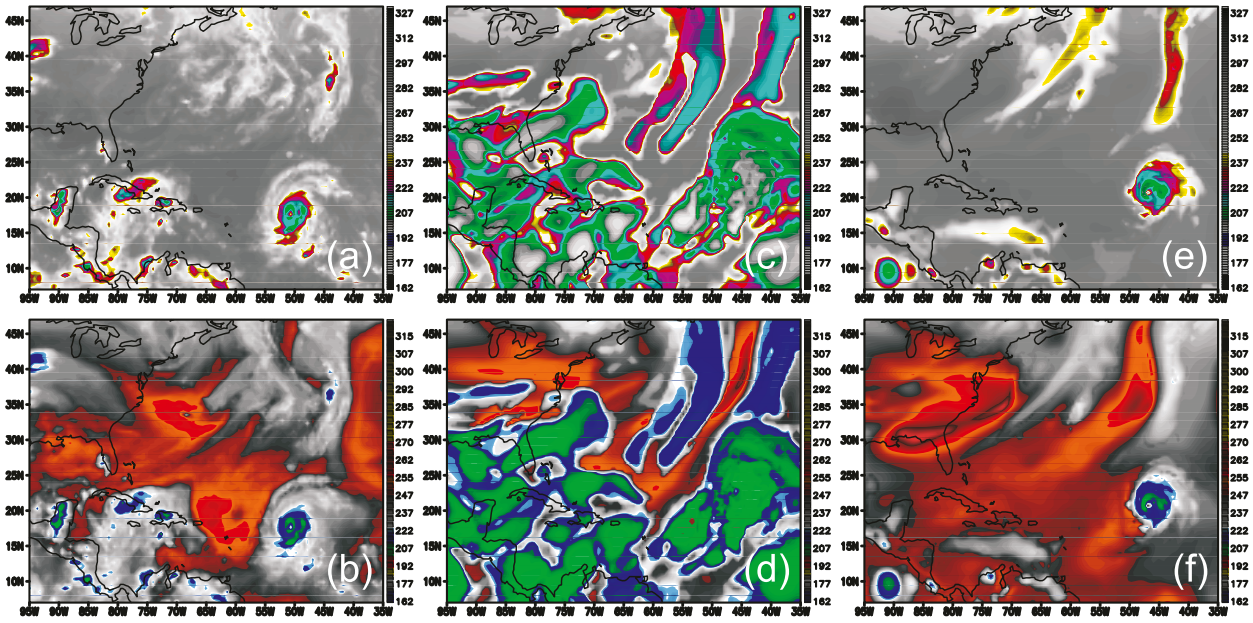

FIG. 9. Observed *GOES-13* (a) CH4 and (b) CH3 Tb (K). (c),(d)–(e),(f) As in (a),(b) but for synthetic Tb from the control and Thompson simulations, respectively. All images are for D1 120-h forecasts, valid at 0000 UTC 14 Sep 2010.

observations. The control experiment has a peak coverage of $\sim 1 \times 10^6\,\text{km}^2$ at very cold Tb, ranging from $-80°$ to $-40°$C, whereas *GOES-13* CH4 observations have nearly zero area in this range. On the warm Tb side between $-10°$ and 30°C, the observations indicate an area reaching $\sim 3 \times 10^6\,\text{km}^2$ around 19°C. The control experiment has a much reduced area of the warm Tb, with only about ½ of the observed at 19°C. The Thompson experiment has much greater areal coverage of 19°C, nearly $5.5 \times 10^6\,\text{km}^2$. The Thompson scheme effectively removes the area of very cold Tb seen in the control simulation mainly because it generates a much lower amount and coverage of cloud ice using the Cooper IN formulation. The contrast in the Tb distribution between the control and Thompson experiments can also be described in the cumulative distribution function (CDF) of Tb (Grasso et al. 2008). The large areal coverage of lower Tb in the control simulation results in much higher CDF values of lower Tb than the Thompson simulation (Fig. 11b). The median value of Tb in the control experiment occurs at $-48°$C, whereas the Thompson median is 17°C and *GOES-13* is 12°C. The Thompson scheme corrects the large deviation from the control and shifts the CDF much closer to the observations. The examination of the synthetic satellite imagery both qualitatively and quantitatively provides further evidence that the Thompson scheme corrects the upper-level cloud ice and temperature overestimated by the control simulation.

b. *Evaluation of track and intensity forecasts for 15 TCs*

Track and intensity forecasts for the 15 TCs (see Table 1) are verified using the best-track data. The homogenized samples for the control and Thompson simulations contain 195 cases at the initialization time and decrease gradually to 79 cases at 120 h (Fig. 12a). The two sets of simulations have the same track forecast errors for the first two days. Beyond that the Thompson track errors are slightly smaller than the control. These differences are not statistically significant based on paired sample Student's *t* tests with adjustments for serial dependence (Wilks 2006). A consistent feature in track errors between the two sets is that the forecast TC locations tend to lag behind and shift to the right of the observed tracks. This can be seen clearly in the decomposition of the track forecast errors relative to the storm motion direction (Fig. 12b). The mean errors (ME) in the cross-track direction are all positive (to the right of the observed tracks) at all forecast lead times for the control simulations, exceeding 100 n mi near the end of the 120-h forecasts. The cross-track ME for the Thompson simulations are relatively small (to the right and then to the left of the observed tracks) during the first 3 days. They increase with the forecast lead time over the next two days, reaching 50 n mi by 120 h, about half of that for the control. The along-track ME in both sets lags behind (negative in Fig. 12b), exceeding 100 n mi at 120 h from

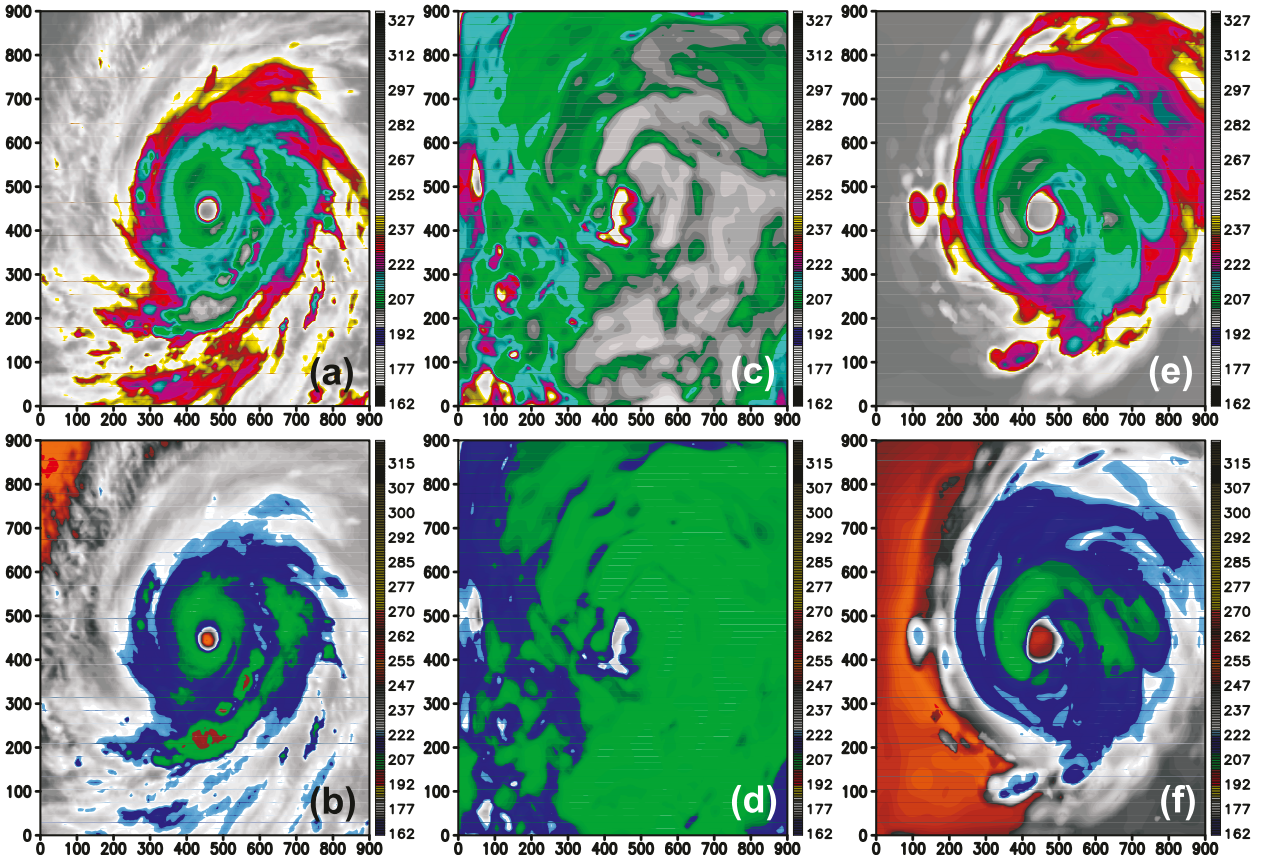

FIG. 10. As in Fig. 9, except for the domain shown in D3 (see Fig. 1). The distance along the *x* axis and *y* axis is in km.

the control, or about twice that of Thompson. The reduction in the mean cross-track and along-track errors in the Thompson simulation is statistically significant for forecast lead times of 72, 96, and 120 h. The improvement seen in the cross-track and along-track bias in the Thompson simulations is consistent with the better-simulated synoptic environment discussed earlier (section 3a).

Mean absolute errors (MAE) and bias were also computed for maximum sustained surface winds (MSW) and minimal sea level pressure (MSLP) for the homogeneous sample. Small differences exist in the MAE of MSW between the control and Thompson simulations (Fig. 12c), but they are not statistically significant. The differences in MSW biases, exceeding 10 kt at times, are however statistically significant for all forecast lead times except 0 and 6 h. The control simulations overestimate MSW (24–120 h) whereas the Thomson simulations underestimate MSW (0–112 h). The overestimated storm intensity by the control simulations is also reflected in the MSLP evolution (Fig. 12d). The negative bias of MSLP increases quickly over the first two days and hovers around −10 hPa over the last 3 days of the control simulation. The Thompson simulations display an MSLP bias between 0 and 5 hPa from 12 to 120 h. The reduction in both MAE and bias of MSLP in the Thompson simulations is statistically significant compared to the control over the forecast period from 36 to 108 h.

TC intensity is arguably most accurately measured in terms of MSLP estimated from flight data, surface observations, and/or dropwindsonde data. However, the potential damage from the storm is usually measured in terms of MSW of which accurate measurement is difficult to obtain. For this reason, the relationship between the MSW and MSLP (wind–pressure relationship) is often used in the operational and research communities to gauge the storm intensity (Knaff and Zehr 2007). Shown in Fig. 13a are the wind–pressure relationships for the two sets of simulations compared with that from the best-track data. At the low wind end (MSW < 60 kt) the wind–pressure relationships from both simulations follow that of the best-track data quite well. As the MSW increases the relationships start to deviate from the observations, with the control simulations showing larger differences than the Thompson simulations. For example, at 930 hPa, the corresponding control MSW

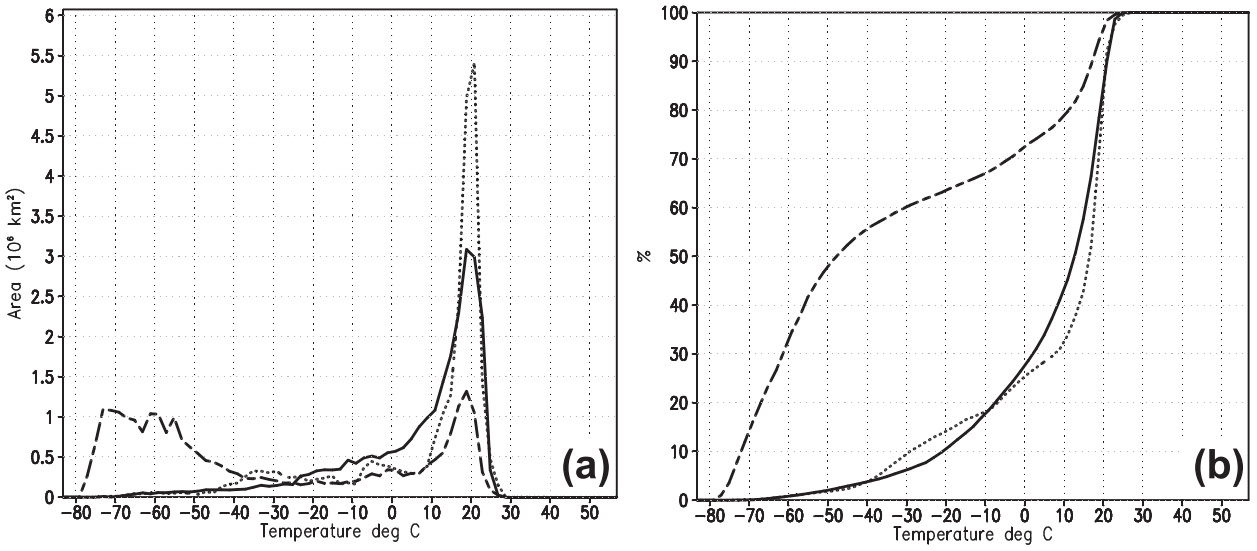

FIG. 11. (a) Areal coverage of Tbs at 0000 UTC 14 Sep 2010 in D1 for *GOES-13* CH4 observations (solid) and the synthetic Tbs from the control (dashed) and Thompson (dotted) simulations at 120 h. (b) As in (a), but for the Tb cumulative distribution function (CDF).

are ~114 kt (cat-3), much lower than ~130 kt (cat-4) from the best-track data. The differing intensities are also examined in terms of intensity-relative frequency distribution (Fig. 13b). The sample size from the Thompson simulations is closer to that in the best-track data than the control simulations for storms of a wide range of intensities (40–110 kt). Both simulations have too many storms in the cat-1 and cat-2 ranges, and too few storms in the cat-4 range. For the TS range, the sample sizes from Thompson are close to those from the best-track data, whereas the control simulation produced too few weak storms. This is another indication that the control tends to overpredict TC intensity.

5. [illegible]

The impacts of microphysical schemes on the forecasts of TC environments, track, and intensity for 15 TCs have been systematically examined for the modified R-H and Thompson schemes in COAMPS-TC. The modified R-H scheme is similar to many other single-moment bulk schemes (Lin et al. 1983; Rutledge and Hobbs 1983), containing five hydrometeor species (cloud water, ice, rain, snow, and graupel). The Thompson scheme is newly designed with a two-moment treatment of ice and rain and one-moment treatment of cloud water, snow, and graupel. Our nearly two months of synoptic simulations point to several noteworthy differences between these two schemes. The upper-level cloud ice produced by the control simulations is up to two orders of magnitude greater than in the Thompson scheme. The main reason for the overabundant cloud ice stems from the choice in the ice nucleation parameterization. The high concentration of ice particles prescribed by the Fletcher formulation at cold temperatures (<-30°C) in the modified R-H scheme leads to the much higher cloud ice concentration compared to the Thompson scheme, which adopts the Cooper ice crystal number formation. A 1°–2°C warm bias, occurring near the 300-hPa level in the control experiment, is not present with the Thompson scheme. The sensitivity test using the Cooper formulation and the test that deactivated the cloud ice–radiation interaction suggest that the upper-level warm bias is associated with the longwave radiative heating at the base of the ice cloud layer. The impact of the two microphysical schemes is also reflected in the extension of the 500-hPa subtropical high—an important parameter controlling the large-scale steering flow for TC tracks. The Thompson scheme enhanced the subtropical high by 10–20 m on average during the 120-h simulation period and prevented the northward retreat of the southern edge of the subtropical high seen in the control simulations.

Consistent with their impacts on the synoptic environment, the two schemes resulted in notable differences in the track forecasts for 15 Atlantic storms of the 2010–11 seasons. The Thompson scheme helps significantly reduce rightward cross-track and slow along-track biases compared to the control simulations, especially over the late forecast lead time (48–120 h). The occurrence of overintensified storms in the control forecasts is much reduced in the Thompson forecasts, especially in terms of MSLP. Such correction leads to a better wind–pressure relationship derived from the Thompson forecasts than

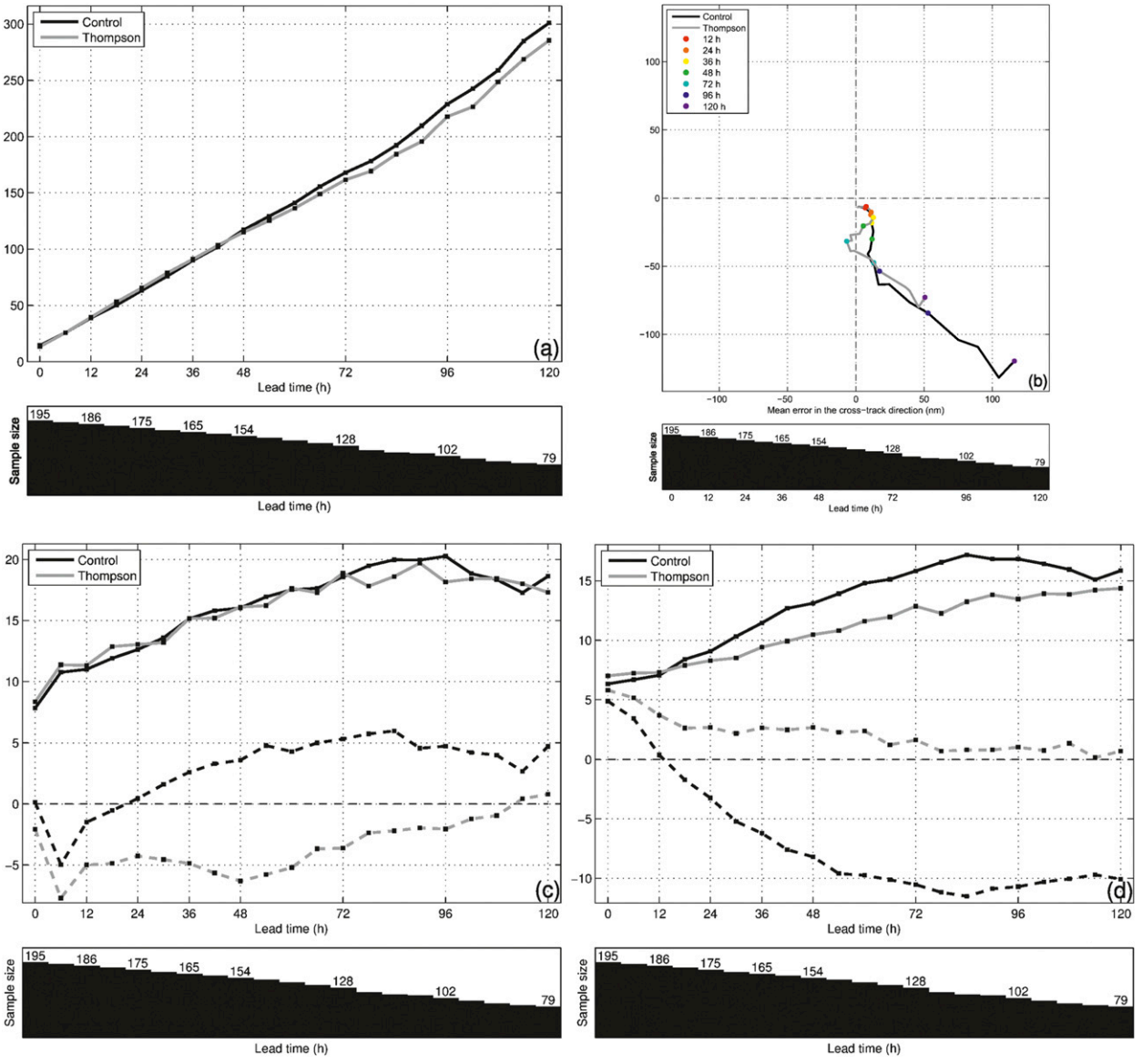

FIG. 12. (a) Track forecast errors (n mi) averaged for the 15 TCs from the control simulations (black) and the Thompson simulations (gray). The lower part contains sample size for the corresponding forecast lead times. (b) As in (a), but for the decomposition of track forecast errors relative to the storm motion direction. The *y* axis shows the along-track error (positive for moving faster than the observed TCs). The *x* axis shows the cross-track errors (positive for the rightward bias of the forecast tracks relative to the observed). The color dots mark forecast lead times (h). (c) Mean absolute errors (solid lines) and bias (dashed) for maximum surface sustained winds (kt) of 15 TCs homogenized for the control (black) and Thompson (gray) experiments. The lower part contains the sample size for corresponding forecast lead times. (d) As in (c), but for the minimal sea level pressure (hPa).

from the control. The Thompson forecasts also increased the relative frequency of weaker storms (TS and cat-1 and -2 hurricanes).

The synthetic satellite imagery from the control experiment of Hurricane Igor clearly shows the low brightness temperature (for CH3 and CH4) associated with the widespread cloud ice over most of the 45-km domain. The Thompson simulation produced much improved brightness temperatures that are close to the satellite observations. In the inner nest with 5-km grid spacing, the Thompson scheme made it possible to examine the inner core structure (i.e., the eye size, orientation of the rainband). The median value of Tb of CH4 from the control simulation occurs at −48°C, which is much lower than the median Tb from both the Thompson simulation (17°C) and the observed (12°C). Applying the synthetic

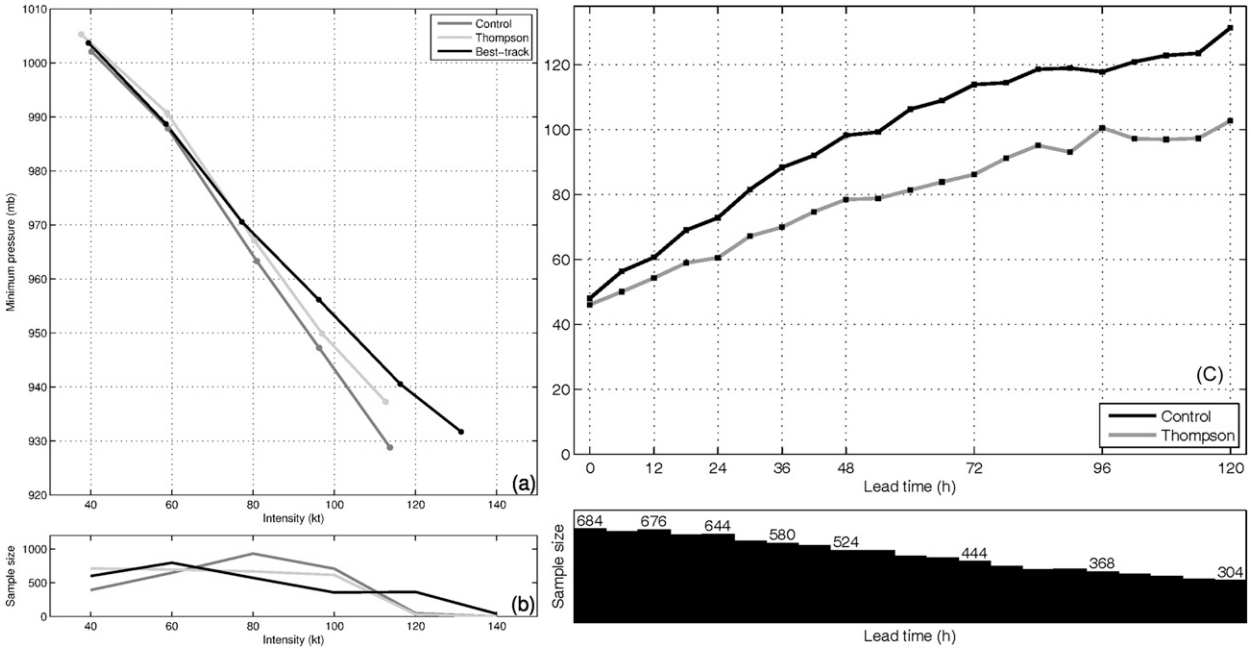

FIG. 13. (a) Minimum surface pressure (hPa) as a function of surface maximum winds (kt) for the best-track data (black), and the control (gray) and the Thompson forecasts (light gray). (b) As in (a), but for the intensity-relative frequency distribution. (c) Average wind radii of 34-kt surface winds for different forecast lead times from the control (black) and the Thompson forecasts (gray); the lower part contains the sample size for corresponding forecast lead times.

satellite imagery in both quantitative and qualitative analyses helped to pinpoint the issue of excessive upper-level cloud ice in the modified R-H microphysics scheme and show its potential use by scheme developers to diagnose problems related to specific microphysical processes. The Thompson scheme requires substantially more computing time (by ~40%) than the modified R-H scheme and hence its application to real-time forecasts is limited. A newly developed single-moment scheme has been implemented in COAMPS-TC and in use in the real-time forecasts since the 2012 hurricane season. This scheme also reduces substantially the upper-level cloud ice and temperature bias seen in the control simulations. A full evaluation of the scheme is underway.

Several issues need further investigation. Improved understanding and representation of the ice nucleation process for TC cases require increased upper-level in situ measurements of cloud ice particles. Observations are also needed to evaluate distribution (especially in the vertical) of hydrometeors. While our focus is on the ice phase clouds, it is recognized that the impact from difference in other microphysical species can play roles in modulating storm intensity and structure, especially at higher resolution (grid spacing < 5 km). Interactions between various physical processes, such as the cloud ice–radiation interaction, turbulence, and air–sea interaction, are also important. Even greater biases are seen at upper levels when we replaced the Fu–Liou radiation scheme with the Harshvardhan et al. (1987) scheme. Further research is needed to improve coupling the radiation parameterizations with the microphysical schemes with radiative effective size of clouds specific to the microphysical scheme. The different wind–pressure relationships between the control and Thompson simulations suggest the sensitivity of the storm structure to the microphysical parameterizations. One example of the TC structure forecasts issued by the National Hurricane Center is the radius of the surface 34-kt winds (R34 hereafter) for four geographical quadrants surrounding the TC center. The R34 values represent the maximum radial extent of the gale-force wind. As shown in Fig. 13c, the R34 values averaged for all four quadrants for the Thompson experiments are smaller than those from the control experiments. This systematic difference in the storm structure is statistically significant. Further examination of such impacts will be presented in a follow-up study that draws comparisons between the model composites and composites from the Doppler radar observations and other conventional observational data.

Acknowledgments. This research was supported by the Office of Naval Research Program Element 0601153N and NOAA HFIP. We are also grateful to

the computational resource and support provided by the Department of Defense (DoD) High Performance Center.

REFERENCES

Bikos, D., and Coauthors, 2012: Synthetic satellite imagery for real-time high-resolution model evaluation. *Wea. Forecasting,* **2 ,** 784–795.

Black, R. A., and J. Hallett, 1986: Observations of the distribution of ice in hurricanes. *J. Atmos. Sci.,* **43,** 802–822.

Black, P. G., and Coauthors, 2007: Air–sea exchange in hurricanes: Synthesis of observations from the Coupled Boundary Layer Air–Sea Transfer Experiment. *Bull. Amer. Meteor. Soc.,* **,** 357–374.

Braun, S. A., 2002: A cloud-resolving simulation of Hurricane Bob (1991): Storm structure and eyewall buoyancy. *Mon. Wea. Rev.,* **130,** 1573–1592.

Chan, J. C.-L., and W. M. Gray, 1982: Tropical cyclone movement and surrounding flow relationship. *Mon. Wea. Rev.,* **110,** 1354–1374.

——, J. Shi, and K. S. Liu, 2001: Improvements in the seasonal forecasting of tropical cyclone activity over the western North Pacific. *Wea. Forecasting,* **16,** 491–498.

Chen, H., D.-L. Zhang, J. Carton, and R. Atlas, 2011: On the rapid intensification of Hurricane Wilma (2005). Part I: Model prediction and structural changes. *Wea. Forecasting,* **26,** 885–901.

Chen, J.-H., M. S. Peng, C. A. Reynolds, and C.-C. Wu, 2009: Interpretation of tropical cyclone forecast sensitivity from the singular vector perspective. *J. Atmos. Sci.,* **66,** 3383–3400.

Clark, A. J., and Coauthors, 2012: An overview of the 2010 Hazardous Weather Testbed Experimental Forecast Program Spring Experiment. *Bull. Amer. Meteor. Soc.,* **3,** 55–74.

Colle, B. A., K. J. Westrick, and C. F. Mass, 1999: Evaluation of MM5 and Eta-10 precipitation forecasts over the Pacific Northwest during the cool season. *Wea. Forecasting,* **14,** 137–154.

Cooper, W. A., 1986: Ice initiation in natural clouds. *Precipitation Enhancement—A Scientific Challenge, Meteor. Monogr.,* No. 43, Amer. Meteor. Soc., 29–32.

Cotton, W. R., and R. A. Anthes, 1989: *Storm and Cloud Dynamics*. Academic Press, 883 pp.

Daley, R., and E. Barker, 2001: NAVDAS: Formulation and diagnostics. *Mon. Wea. Rev.,* **12 ,** 869–883.

DeMott, P. J., and Coauthors, 2011: Resurgence in ice nuclei measurement research. *Bull. Amer. Meteor. Soc.,* **2,** 1623–1635.

Donelan, M. A., B. K. Haus, N. Reul, W. J. Plant, M. Stiassnie, and H. C. Graber, 2004: On the limiting aerodynamic roughness of the ocean in very strong winds. *Geophys. Res. Lett.,* **31,** L18306, doi:10.1029/2004GL019460.

Doyle, J. D., and Coauthors, 2012: Real-time tropical cyclone prediction using COAMPS-TC. *Advances in Geosciences,* Vol. 28, K. Satake, Ed., World Scientific, 15–28.

Emanuel, K. A., 1986: An air–sea interaction theory for tropical cyclones. Part I: Steady-state maintenance. *J. Atmos. Sci.,* **43,** 585–605.

——, 1999: Thermodynamic control of hurricane intensity. *Nature,* **401,** 665–669.

Fairall, C., F. Bradley, D. P. Rogers, J. B. Edson, and G. S. Young, 1996: Bulk parameterization of air–sea fluxes for Tropical Ocean Global Atmosphere Coupled Ocean–Atmosphere Response Experiment. *J. Geophys. Res.,* **101,** 3747–3764.

Ferrier, B. S., 1994: A double-moment multiple-phase four-class bulk ice scheme. Part I: Description. *J. Atmos. Sci.,* **51,** 249–280.

Fierro, A. O., R. F. Rogers, F. D. Marks, and D. S. Nolan, 2009: The impact of horizontal grid spacing on the microphysical and kinematic structures of strong tropical cyclones simulated with the WRF-ARW model. *Mon. Wea. Rev.,* **13 ,** 3717–3743.

Fletcher, N. H., 1962: *The Physics of Rain Clouds.* Cambridge University Press, 390 pp.

Fovell, R. G., K. L. Corbosiero, and H.-C. Kuo, 2009: Cloud microphysics impact on hurricane track as revealed in idealized experiments. *J. Atmos. Sci.,* **66,** 1764–1778.

Grasso, L. D., M. Sengupta, J. F. Dostalek, R. Brummer, and M. DeMaria, 2008: Synthetic satellite imagery for current and future environmental satellites. *Int. J. Remote Sens.,* **2 ,** 4373–4384.

Gray, W. M., and D. J. Shea, 1973: The hurricane's inner core region. II. Thermal stability and dynamic characteristics. *J. Atmos. Sci.,* **30,** 1565–1576.

Harshvardhan, R. Davies, D. Randall, and T. Corsetti, 1987: A fast radiation parameterization for atmospheric circulation models. *J. Geophys. Res.,* **2,** 1009–1016.

Hendricks, E. A., M. T. Montgomery, and C. A. Davis, 2004: The role of ''vortical'' hot towers in the formation of Tropical Cyclone Diana (1984). *J. Atmos. Sci.,* **61,** 1209–1232.

Heymsfield, A. J., A. Bansemer, S. L. Durden, R. L. Herman, and T. P. Bui, 2006: Ice microphysics observations in Hurricane Humberto: Comparison with non-hurricane-generated ice cloud layers. *J. Atmos. Sci.,* **63,** 288–308.

Heymsfield, G., J. Halverson, J. Simpson, L. Tian, and T. P. Bui, 2001: ER-2 Doppler radar investigations of the eyewall of Hurricane Bonnie during the Convection and Moisture Experiment-3. *J. Appl. Meteor.,* **40,** 1310–1330.

Hong, S.-Y., J. Dudhia, and S.-H. Chen, 2004: A revised approach to ice microphysical processes for the bulk parameterization of clouds and precipitation. *Mon. Wea. Rev.,* **132,** 103–120.

Houze, R. A., Jr., F. D. Marks, and R. A. Black, 1992: Dual-aircraft investigation of the inner core of Hurricane Norbert. Part II: Mesoscale distribution of ice particles. *J. Atmos. Sci.,* **4 ,** 943–963.

Jin, Y., W. T. Thompson, S. Wang, and C.-S. Liou, 2007: A numerical study of the effect of dissipative heating on tropical cyclone intensity. *Wea. Forecasting,* **22,** 950–966.

Jorgensen, D. P., 1984: Mesoscale and convective-scale characteristics of mature hurricanes. Part II: Inner core structure of Hurricane Allen (1980). *J. Atmos. Sci.,* **41,** 1287–1311.

Kain, J. S., and J. M. Fritsch, 1990: A one-dimensional entraining/detraining plume model and its application in convective parameterization. *J. Atmos. Sci.,* **4 ,** 2784–2802.

Kasahara, A., 1961: A numerical experiment on the development of tropical cyclone. *J. Meteor.,* **1 ,** 259–282.

Klemp, J. B., and R. B. Wilhelmson, 1978: The simulation of three-dimensional convective storm dynamics. *J. Atmos. Sci.,* **35,** 1070–1096.

Knaff, J. A., and R. M. Zehr, 2007: Reexamination of tropical cyclone wind–pressure relationships. *Wea. Forecasting,* **22,** 71–88.

Li, X., and Z. Pu, 2008: Sensitivity of numerical simulation of early rapid intensification of Hurricane Emily (2005) to cloud microphysical and planetary boundary layer parameterizations. *Mon. Wea. Rev.,* **136,** 4819–4838.

Lin, Y.-L., R. D. Farley, and H. D. Orville, 1983: Bulk parameterization of the snow field in a cloud model. *J. Climate Appl. Meteor.,* **22,** 1065–1092.

Liou, C.-S., and K. D. Sashegyi, 2012: On the initialization of tropical cyclones with a three dimensional variational analysis. *Nat. Hazards,* **63,** 1375–1391.

Liu, C., K. Ikeda, G. Thompson, R. Rasmussen, and J. Dudhia, 2011: High-resolution simulations of wintertime precipitation in the Colorado Headwaters region: Sensitivity to physics parameterizations. *Mon. Wea. Rev.,* **13 ,** 3533–3553.

Liu, M., J. E. Nachamkin, and D. L. Westphal, 2009: On the improvement of COAMPS weather forecasts using an advanced radiative transfer model. *Wea. Forecasting,* **24,** 286–306.

Liu, Y., D.-L. Zhang, and M. K. Yau, 1997: A multiscale numerical study of Hurricane Andrew (1992). Part I: Explicit simulation and verification. *Mon. Wea. Rev.,* **125,** 3073–3093.

Lord, S. J., H. E. Willoughby, and J. M. Piotrowicz, 1984: Role of a parameterized ice-phase microphysics in an axisymmetric, nonhydrostatic tropical cyclone model. *J. Atmos. Sci.,* **41,** 2836–2848.

Louis, J.-F., 1979: A parametric model of vertical eddy fluxes in the atmosphere. *Bound.-Layer Meteor.,* **1 ,** 187–202.

Malkus, J. S., 1958: On the structure and maintenance of the mature hurricane eye. *J. Meteor.,* **15,** 337–349.

——, and H. Riehl, 1960: On the dynamics and energy transformations in steady-state hurricanes. *Tellus,* **12,** 1–20.

McFarquhar, G. M., and R. A. Black, 2004: Observations of particle size and phase in tropical cyclones: Implications for mesoscale modeling of microphysical processes. *J. Atmos. Sci.,* **61,** 422–439.

——, H. Zhang, G. Heymsfield, R. Hood, J. Dudhia, J. B. Halverson, and F. Marks, 2006: Factors affecting the evolution of Hurricane Erin (2001) and the distributions of hydrometeors: Role of microphysical processes. *J. Atmos. Sci.,* **63,** 127–150.

Mellor, G. L., and T. Yamada, 1982: Development of a turbulence closure for geophysical fluid problems. *Rev. Geophys. Space Phys.,* **20,** 851–875.

Meyers, M. P., P. J. DeMott, and W. R. Cotton, 1992: New primary ice-nucleation parameterizations in an explicit cloud model. *J. Appl. Meteor.,* **31,** 708–721.

Milbrandt, J. A., and M. K. Yau, 2005: A multimoment bulk microphysics parameterization. Part I: Analysis of the role of the spectral shape parameter. *J. Atmos. Sci.,* **62,** 3051–3064.

Molthan, A. L., and B. A. Colle, 2012: Comparisons of single- and double-moment microphysics schemes in the simulation of a synoptic-scale snowfall event. *Mon. Wea. Rev.,* **140,** 2982–3002.

Morrison, H., and J. O. Pinto, 2005: Mesoscale modeling of springtime Arctic mixed-phase stratiform clouds using a new two-moment bulk microphysics scheme. *J. Atmos. Sci.,* **62,** 3683–3704.

Nicholls, S., 1984: The dynamics of stratocumulus: Aircraft observations and comparisons with a mixed layer model. *Quart. J. Roy. Meteor. Soc.,* **110,** 783–820.

Pruppacher, H. R., and J. D. Klett, 1978: *Microphysics of Clouds and Precipitation.* D. Reidel, 714 pp.

Reisner, J., R. M. Rasmussen, and R. T. Bruintjes, 1998: Explicit forecasting of supercooled liquid water in winter storms using the MM5 mesoscale model. *Quart. J. Roy. Meteor. Soc.,* **124,** 1071–1107.

Riehl, H., and J. S. Malkus, 1961: Some aspects of Hurricane Daisy, 1958. *Tellus,* **13,** 181–213.

Rogers, R., 2010: Convective-scale structure and evolution during a high-resolution simulation of tropical cyclone rapid intensification. *J. Atmos. Sci.,* **6 ,** 44–70.

——, M. L. Black, S. S. Chen, and R. A. Black, 2007: An evaluation of microphysics fields from mesoscale model simulations of tropical cyclones. Part I: Comparisons with observations. *J. Atmos. Sci.,* **64,** 1811–1834.

Rosenthal, S. L., 1978: Numerical simulation of tropical cyclone development with latent heat release by the resolvable scales I: Model description and preliminary results. *J. Atmos. Sci.,* **35,** 258–271.

Rutledge, S. A., and P. V. Hobbs, 1983: The mesoscale and microscale structure and organization of clouds and precipitation in midlatitude cyclones. VIII: A model for the ''seeder-feeder'' process in warm-frontal rainbands. *J. Atmos. Sci.,* **40,** 1185–1206.

Schultz, P., 1995: An explicit cloud physics parameterization for operational numerical weather prediction. *Mon. Wea. Rev.,* **123,** 3331–3343.

Shen, B.-W., W.-K. Tao, W. K. Lau, and R. Atlas, 2010: Predicting tropical cyclogenesis with a global mesoscale model: Hierarchical multiscale interactions during the formation of Tropical Cyclone Nargis (2008). *J. Geophys. Res.,* **115,** D14102, doi:10.1029/2009JD013140.

Simpson, J., J. Halverson, B. S. Ferrier, W. A. Petersen, R. H. Simpson, R. Blakeslee, and S. L. Durden, 1998: On the role of ''hot towers'' in tropical cyclone formation. *Meteor. Atmos. Phys.,* **6 ,** 15–35.

Thompson, G., R. M. Rasmussen, and K. Manning, 2004: Explicit forecasts of winter precipitation using an improved bulk microphysics scheme. Part I: Description and sensitivity analysis. *Mon. Wea. Rev.,* **132,** 519–542.

——, P. R. Field, R. M. Rasmussen, and W. D. Hall, 2008: Explicit forecasts of winter precipitation using an improved bulk microphysics scheme. Part II: Implementation of a new snow parameterization. *Mon. Wea. Rev.,* **136,** 5095–5115.

Wang, S., Q. Wang, and J. Doyle, 2002: Some improvement of Louis surface flux parameterization. Preprints, *15th Symp. on Boundary Layers and Turbulence,* Wageningen, Netherlands, Amer. Meteor. Soc., 547–550.

Wang, Y., 2002: An explicit simulation of tropical cyclones with a triply nested movable mesh primitive equation model: TCM3. Part II: Model refinements and sensitivity to cloud microphysics parameterization. *Mon. Wea. Rev.,* **130,** 3022–3036.

Wilks, D., 2006: *Statistical Methods in the Atmospheric Sciences.* 2nd ed. Academic Press, 677 pp.

Willoughby, H. E., 1998: Tropical cyclone eye thermodynamics. *Mon. Wea. Rev.,* **126,** 3053–3067.

——, 2009: Diabatically induced secondary flows in tropical cyclones. Part II: Periodic forcing. *Mon. Wea. Rev.,* **13 ,** 822–835.

——, H.-L. Jin, S. J. Lord, and J. M. Piotrowicz, 1984: Hurricane structure and evolution as simulated by axisymmetric, nonhydrostatic numerical model. *J. Atmos. Sci.,* **41,** 1169–1186.

Wu, C.-C., J.-H. Chen, P.-H. Lin, and K.-H. Chou, 2007: Targeted observations of tropical cyclone movement based on the adjoint-derived sensitivity steering vector. *J. Atmos. Sci.,* **64,** 2611–2626.

Zhu, T., and D.-L. Zhang, 2006: Numerical simulation of Hurricane Bonnie (1998). Part II: Sensitivity to varying cloud microphysical processes. *J. Atmos. Sci.,* **63,** 109–126.

Zipser, E. J., 2003: Some views on ''hot towers'' after 50 years of tropical field programs and two years of TRMM data. *Cloud Systems, Hurricanes, and the Tropical Rainfall Measuring Mission (TRMM)—A Tribute to Dr. Joanne Simpson, Meteor. Monogr.,* No. 51, Amer. Meteor. Soc., 49–58.